Inverter-machine parametric co-design for energy efficient electric drives

Jaedon Kwak, Alberto Castellazzi
Kyoto University of Advanced Science
Ukyo Ward, Yamanouchi Gotandacho, 18
Kyoto, Japan
Tel.: +81 / 7033013693.
E-Mail: 2020md02@kuas.ac.jp

Keywords

«Optimal efficiency drive», «Wide Bandgap devices», «Multi-level inverters», «Silicon Carbide (SiC)», «Hybrid Electric Vehicle (HEV)»

Abstract

This paper presents the development of a unified parametric machine-inverter design framework targeted at energy efficiency optimization that is taking into account the most frequent operational conditions and the integral of the power losses over time. A case study is conducted with 400V-30kW ISG in hybrid electric vehicle application. For 3L-ANPC with wide band gap device, various switching frequencies, and different type of topologies and PWM strategies are compared with respect to energy loss in both inverter and machine. The machine design methodology is presented considering interactive effect between inverter and machine. As a result, proposed design has an advantage of energy loss compared to conventional design. The activity will contribute to drive progress beyond state-of-the-art in key application domains.

Introduction

Electrical machine drive systems(ED) are a key point for electric vehicle(EV) and hybrid electric vehicle(HEV) applications. To achieve satisfactory operational range, energy consumption must be low: that is, the ED must be efficient and lightweight. With this goal, many studies have been conducted to increase energy efficiency in the fields of inverters and machines. In general, conventional design of 3-phase inverter for ED uses 2-level half bridge topology with Si-IGBT for their power device. With high demand collector-emitter current, it can be challenging to adopt high switching frequency due to the high heat-generation of the Si-IGBT. Wide-band-gap(WBG; silicon carbide, SiC; gallium nitride, GaN) based power conversion is well known to enable increased power density and efficiency as a result of higher current density of the semiconductors, smaller module footprints, higher switching frequencies and operational temperature [1-3]. Compared to 2-level inverters, multilevel inverter topologies such as advanced neutral point clamped(ANPC) inverter offers several advantages in terms of efficiency and current harmonics [4-6]. In machine design for ED, permanent magnet synchronous machine(PMSM) is wide spread and vastly used due to its high power density and efficiency [7], [8]. These design parameters not only affect the energy efficiency of each inverter and machine, but also affects each other mutually. In [9] and [10], authors investigate that machine's iron loss and magnet eddy current loss are influenced by the PWM waveform depending on the inverter switching frequency. By increasing switching frequency with SiC inverter, the losses and temperature of motor can be reduced in [11]. Though design variables of each inverter and machine can affect mutually, research has hitherto largely targeted the machine and the inverter independently. Besides, few studies have considered integrated design considering interactive effects at initial design stage. For this reason, unified parametric machine-inverter co-design must be conducted for minimizing energy consumption of system. System performance is optimized taking into account the prevalent load, that is the statistically most relevant operational condition from application driving cycle.
In this paper, unified framework enabling for energy efficient optimization is proposed with a case study of 400Vdc-30kW integrated starter generator(ISG) and their drive system in plug-in hybrid vehicle. A

parametric design method using some of major design variables of machine and inverter is presented. A co-simulation considering inverter-machine mutual effect is conducted in order to calculate energy consumption of system during driving cycle, represented by US06.

Approach and methodology

Calculation energy loss consumption during driving cycle

Initial design specification of 400Vdc-30kW belt driven ISG model is shown in Table I. To calculate energy loss consumption during driving cycle, US06 driving cycle is used. Vehicle profile and machine profile of US06 is presented in Fig. 1.

Table I: Specification of 400Vdc-30kW ISG model

Item		Specification
Power / Torque		30kW (motoring & generating) / ±50Nm
DC-link voltage / max. phase current		400Vdc / 180Arms
Max. speed		18,000 rpm
Pulley ratio		3:1
Inverter	Inverter topology	2L- half bridge 3-phase inverter with Si-IGBT
	Switching frequency	10 kHz
Machine	Motor type	IPMSM
	Pole / Slot	8 / 48
	Outer Diameter / Stack Length [mm]	130mm / 55mm
	Winding type	Rectangular wire / hair-pin winding
	Magnet	NdFeB

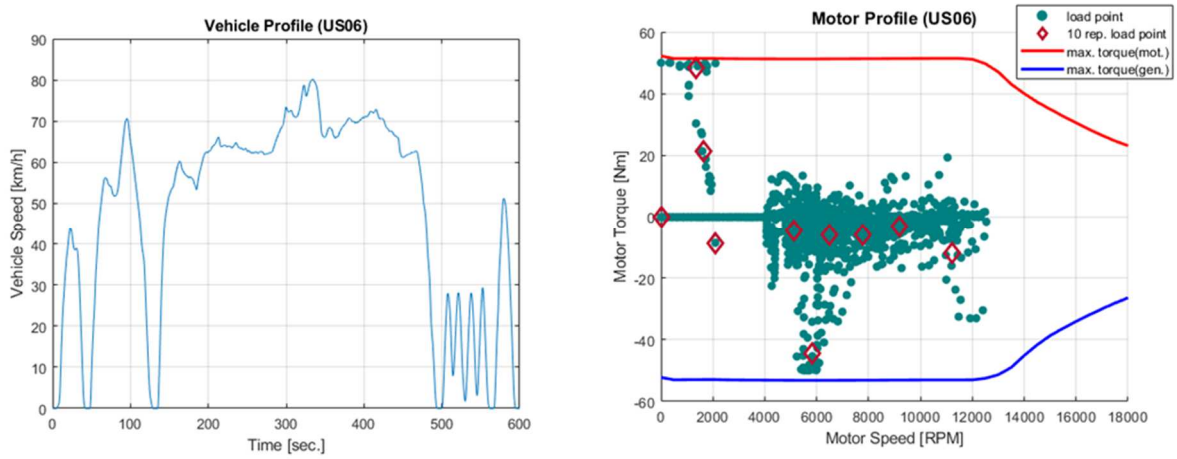

(a) (b)

Fig. 1: US06 driving cycle : (a) vehicle profile (b) ISG profile with S-T curve and 10 representative load point

In [12], The subregions of each load point can be devided and representative equivalent load points are calculated by equation (1)-(3), where N_i represents the number of points in the ith subregion, Emi is the energy of ith region, n_{mci} and T_{mci} represents speed and torque in the energy gravity center point.

$$E_{mi} = \sum_{j=1,2,\ldots}^{N_i} E_{mij} \quad (1)$$

$$n_{mci} = \frac{1}{E_{mi}} \sum_{j=1,2,\ldots}^{N_i} E_{mij} n_{mij} \tag{2}$$

$$T_{mci} = \frac{1}{E_{mi}} \sum_{j=1,2,\ldots}^{N_i} E_{mij} T_{mij} \tag{3}$$

The number of subregions influences the accuracy of the representative points. In this paper, 10 representative points are sufficient to represent the entire cycle, which is shown in Table II.

Table II: 10 representative points of US06 driving cycle

No.	Time [sec.]	Speed [rpm]	Torque [Nm]
1	1.2	1640.9	21.2
2	2.7	1342.4	48.3
3	8.6	5815.1	-44.5
4	12.9	11215.9	-11.9
5	22.4	2094.8	-8.6
6	36.6	9186.7	-3.3
7	42.0	7789.6	-5.9
8	77.9	6490.6	-6.0
9	195.0	5105.2	-4.5
10	200.7	0.0	0.0

Design parameters

Given machine type and inverter, design optimization can exploit the following parameters:

1) Number of levels(N_L): higher N_L yields voltage waveforms closer to pure sinus, improving machine efficiency due to better harmonics, and decreasing voltage endurance level for each power device; however, it can imply lower inverter efficiency due to larger switch number, on top of a more complex design.
2) Switching frequency(f_s): higher f_s reduces output current harmonics, and losses of machine can be decreased, especially at high-speed region. But it causes high inverter switching loss.
3) PWM strategy: depending on inverter topology, current ripple and inverter losses are influenced by PWM strategies. Besides, current ripple impacts on machine losses.
4) Machine pole number(n_p) and stator number of series turns(n_T): higher n_p increase power density with low magnetic reluctance; it requires higher f_s to keep stable controllability. n_T impact on power density as well as stator inductance, that is related to current ripple.

The governing design equations for the inverter loss that comprised conduction and switching loss can be expressed as

$$P_{cond,IGBT} = I(\theta)V_{ce} + I(\theta)^2 R_{ce} \tag{4}$$

$$P_{cond,\mathrm{Diode}} = I(\theta)V_f + I(\theta)^2 R_f \tag{5}$$

$$P_{cond,\mathrm{MOS}} = I(\theta)^2 R_{ds} \tag{6}$$

$$P_{sw,\mathrm{IGBT}} = \left[E_{on,\mathrm{IGBT}}(I,T,V_{DC}) + E_{off,\mathrm{IGBT}}(I,T,V_{DC})\right] \cdot f_s \tag{7}$$

$$P_{sw,\mathrm{MOS}} = \left[E_{on,\mathrm{MOS}}(I,T,V_{DC}) + E_{off,\mathrm{MOS}}(I,T,V_{DC})\right] \cdot f_s \tag{8}$$

$$P_{rec,\mathrm{Diode}} = E_{rec,diode}(I,T,V_{DC}) \cdot f_s \tag{9}$$

$I(\theta)$ is the current flowing through switches, V_{ce} and V_f are the initial saturation voltage drop of IGBT and diode, R_{ce}, R_f, and R_{ds} are the on-state resistance of IGBT, diode, and MOSFET. $E_{on,\mathrm{IGBT}}(I,T,V_{DC})$ $E_{off,\mathrm{IGBT}}(I,T,V_{DC})$, $E_{on,\mathrm{MOS}}(I,T,V_{DC})$, and $E_{off,\mathrm{MOS}}(I,T,V_{DC})$ represent the energy per unit switching on and off state of IGBT and MOSFET, and $E_{rec,diode}(I,T,V_{DC})$ is the reverse recovery energy per unit switching period of diode.
For the machine, the copper loss and iron loss can be expressed as

$$P_{copper} = 3i_S^2 \cdot R_{copper} \tag{10}$$

$$P_{iron} = P_{hyst} + P_{eddy} = k_{minor} k_h(f,B_m) \cdot f \cdot B_m^2 + \sum k_e(f,B_m) \cdot f_n^2 \cdot B_{m\_n}^2 \tag{11}$$

$$k_{minor} = 1 + k \frac{1}{B_m} \sum \Delta B_n \tag{12}$$

with R_{copper} the stator resistance of one phase, that is dependent on frequency due to AC skin and proximity effect [13], and i_S the stator current; $k_{h,e,minor}$ are parameters for hysteresis, eddy-current losses and B_m is flux density, f_n and B_n is harmonic component of frequency and flux density [9].

Design with co-simulation

Inverter design

To investigate multi-level topology, 3-level ANPC inverter are taken into account. By rationally selecting the zero-state loop, the loss balance of each devices in 3L-ANPC can be achieved. In addition, the flexible commutation mode of the ANPC topology also provides the possibility for hybrid configuration of power devices [4-6]. In this paper, two different topologies are presented shown in Fig. 2.

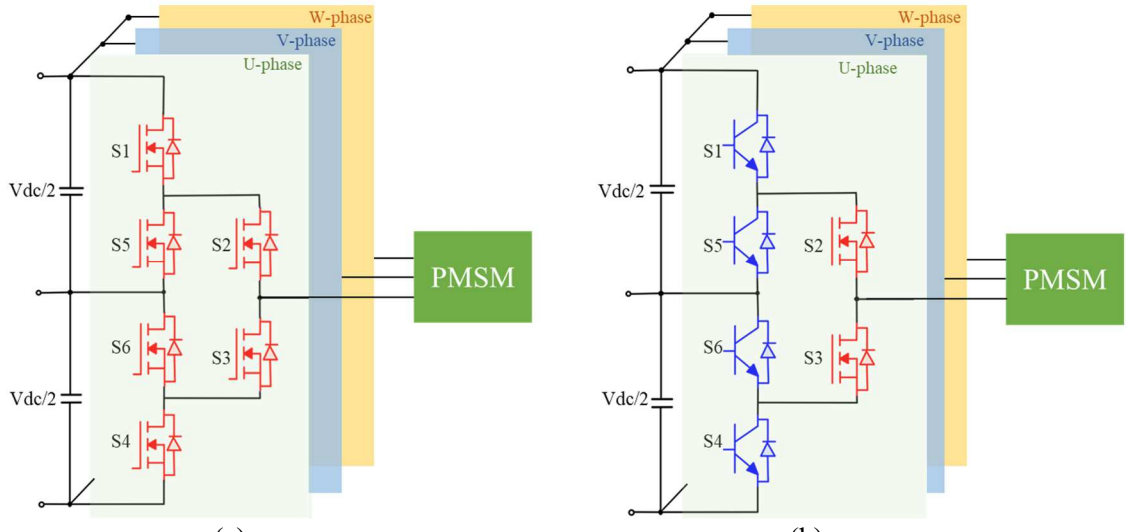

Fig. 2: 3L-ANPC topologies : (a) All SiC-MOSFET; (b) Hybrid Si-IGBT & SiC-MOSFET

The proposed PWM strategies are presented in Fig. 3 and Fig. 4. In PWM1, the current flows in two parallel paths at zero-states: S5-S2 and S6-S3, that leads the low conduction losses at zero-states [1]. Only two devices(S2, S3) switches at switching frequency and the others switch at line frequency, that leads the low switching losses with 4 devices except S2, S3 in PWM2 [4], [6]. This strategy is suitable for hybrid topology due to little switching loss on the 4 IGBT devices.

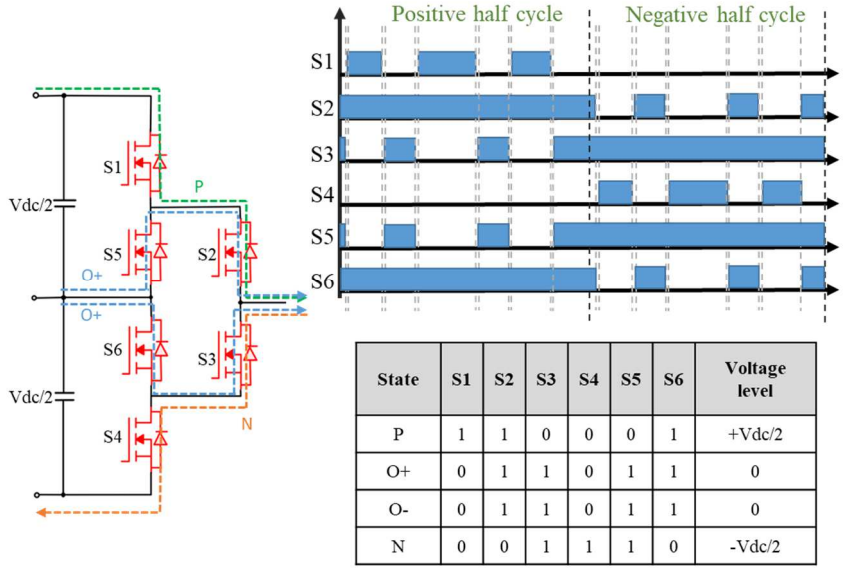

State	S1	S2	S3	S4	S5	S6	Voltage level
P	1	1	0	0	0	1	+Vdc/2
O+	0	1	1	0	1	1	0
O-	0	1	1	0	1	1	0
N	0	0	1	1	1	0	-Vdc/2

(a) (b)

Fig. 3: PWM1 strategy: (a) current loop for each state; (b) switching signal and states

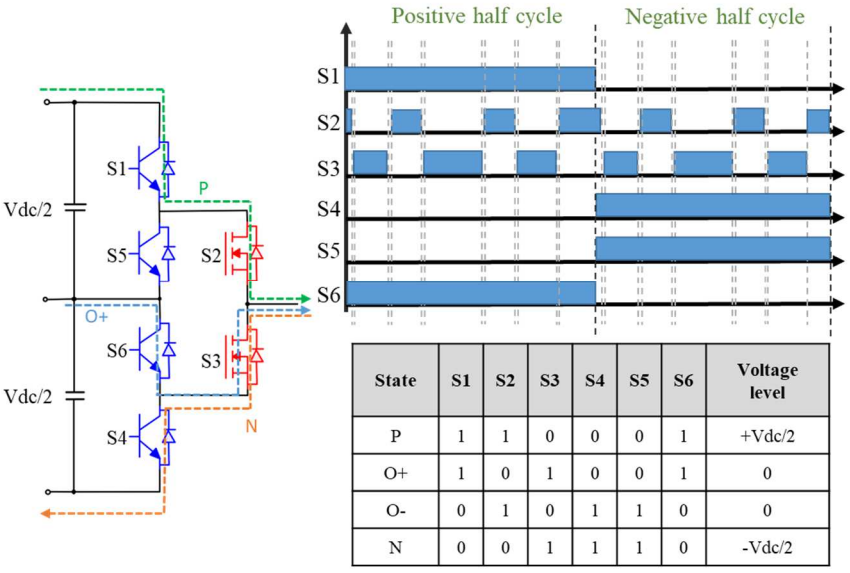

State	S1	S2	S3	S4	S5	S6	Voltage level
P	1	1	0	0	0	1	+Vdc/2
O+	1	0	1	0	0	1	0
O-	0	1	0	1	1	0	0
N	0	0	1	1	1	0	-Vdc/2

(a) (b)

Fig. 4: PWM2 strategy: (a) current loop for each state; (b) switching signal and states

The simulation model is composed of a closed loop with PI current controller, PWM strategies, 3level-ANPC model, and PMSM model. For PMSM model, the tabulated parameters interpreted as FEM based at the corresponding load point are used. Inverter model have power devices refer to Table III. The losses are compared with a combination of two topologies and two PWM strategies at two different load points in Table II; 1) load 2: a relatively large current excitation at low speed, and 2) load 4: a relatively small current excitation at a high speed.

Table III: Power device specification

Topology	Device	Part No.	V_{ce} / V_{ds}	I_c / I_d	Remarks
2L-HB	Si-IGBT/Diode	Infineon - IKQ75N120CT2	1200	75	3-parallel
3L-ANPC	Si-IGBT/Diode	Infineon – AIKQ120N60CT	600	120	2-parallel
	SiC-MOSFET	Wolfspeed - C3M0015065D	650	120	2-parallel

Speed[rpm]	Torque[Nm]	Current [A]	Voltage[V]
1342.4	48.3	235.0	55.4

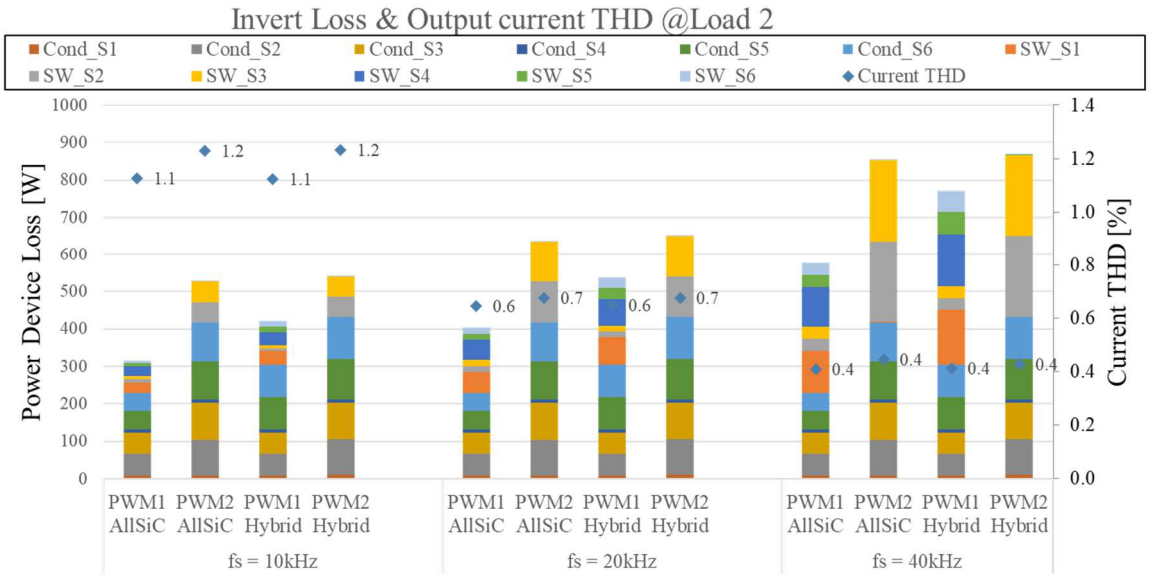

Fig. 5: Comparison of 3L-ANPC inverter losses at load2 in Table II

Speed[rpm]	Torque[Nm]	Current [A]	Voltage[V]
11,215.9	-11.9	57.9	291.2

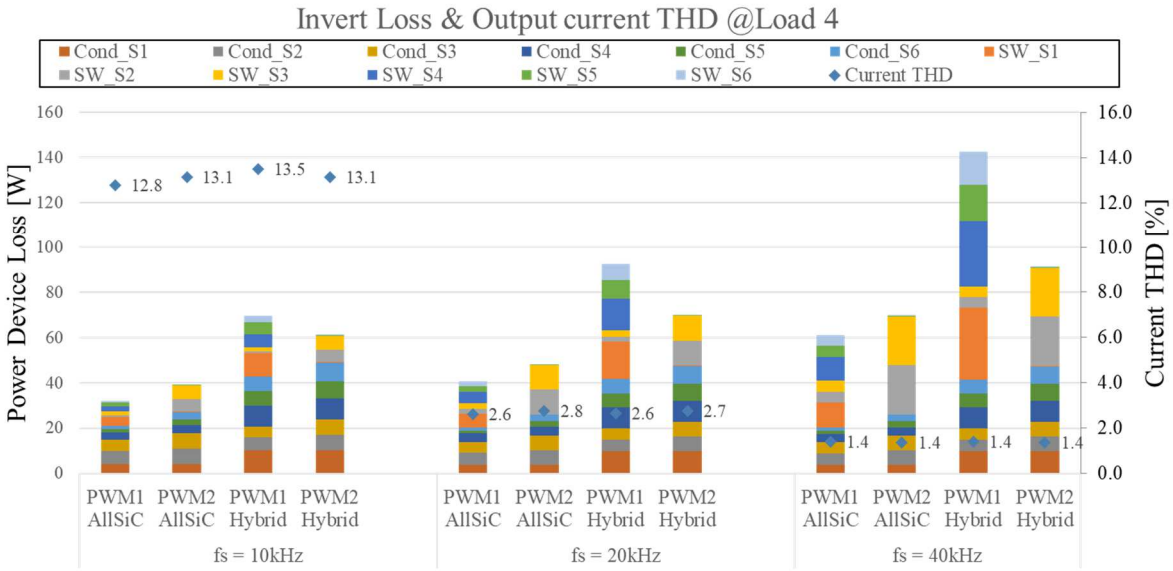

Fig. 6: Comparison of 3L-ANPC inverter losses at load4 in Table II

The results of comparison of the inverter loss are illustrated in Fig. 5, and Fig. 6. The quality of the output current waveform that is represented by total harmonic distortion(THD) is dependent on f_s, and not greatly effected by 2 PWM strategies. THD of output current is calculated by equation (13) where I_n is amplitude of current harmonics.

$$THD = \frac{\sqrt{I_2^2+I_3^2+I_4^2+\cdots}}{I_1} \tag{13}$$

In low speed and high current region that is such as load 2 in Table II, inverter losses of PWM1 are smaller than one of PWM2 with both topologies as Fig. 5. In contrast, PWM2 is more efficient in hybrid

topology in high speed and low current region such as load 4 in Table II, as illustrated in Fig. 6. As results, PWM2 has an advantage in high-speed region where switching loss is dominant, while PWM1 is more efficient in low speed where conduction loss is dominant.
For the machine, especially in high region such as load 4, the losses are affected by the fs, that is the harmonic component, THD of output current waveform as Fig. 7.

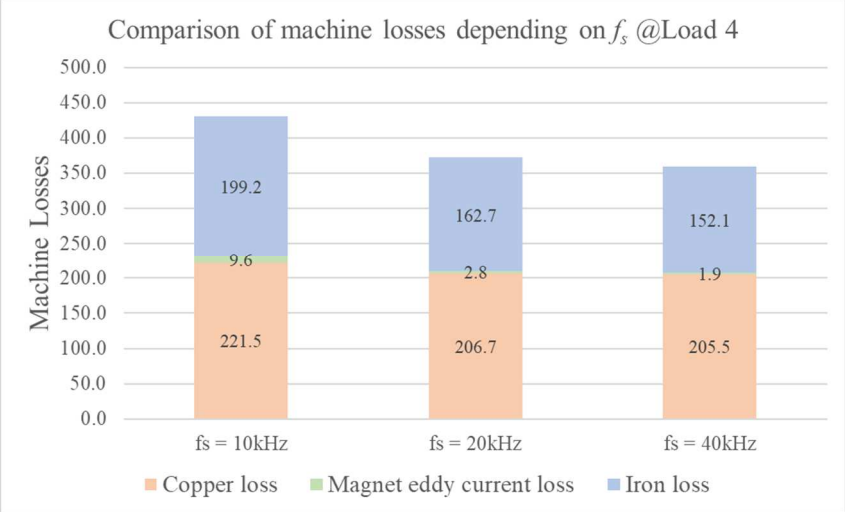

Fig. 7: Comparison of machine losses depending on f_s in PWM1 hybrid topology at load 4 in Table II

Machine design considering inverter parameter

As far as the machine is concerned, the discussion can actually be easily extended to include additional interrelation between f_s and other design parameters. For the sake of illustration, here the possibility to increase the machine number of poles when f_s is increased is considered. When designing the machine, the maximum number of poles, n_{p_max} can be expressed as follows.

$$n_{p\_max} = 120 \times \frac{f_s}{N_{max} \times m_f} \tag{14}$$

N_{max} is the highest rotational speed of the machine, in rpm, and m_f the frequency modulation index, that is, the ratio of switching to fundamental electrical frequency. Thus, by increasing f_s, n_{p_max} can also be increased. In [14] and [15] , increasing pole number of PMSM offers advantages of power density and efficiency. As the number of poles increases, the fundamental flux per pole Φ_1 decreases at the same air-gap flux density B_g as equation (15) where D_r is rotor diameter, and l_{stk} is effective stack length. Thinner yoke thickness are allowed due to reduced magnetic flux per pole and shorter magnetic flux paths. That means high power density at given size by increasing air-gap flux density.

$$\Phi_1 = B_g \cdot \frac{\pi D_r l_{stk}}{n_p} \tag{15}$$

For the number of series turns per phase n_T, expressed by equation (16)-(18).

$$E_{ph} = \frac{P_{max}}{3 i_{s\_max}} \text{ (@base speed)} \tag{16}$$

$$E_{ph} = \frac{2\pi}{\sqrt{2}} \cdot f k_{w1} n_T \Phi_1 = \frac{\pi^2}{\sqrt{2}} \frac{\omega_m}{60} k_{w1} n_T B_g D_r l_{stk} \tag{17}$$

$$n_T = \frac{P_{max}}{3 i_{s\_max}} \cdot \frac{\sqrt{2}}{\pi^2} \cdot \frac{60}{\omega_m k_{w1} B_g D_r l_{stk}} \tag{18}$$

E_{ph} is the phase electro-motive force at base speed, P_{max} and i_{s_max} are the maximum value of power and phase rms current, k_{w1} is the fundamental harmonic winding factor, and ω_m is the mechanical base speed of machine for rpm. Furthermore, n_T affects output current harmonics. The stator inductance is proportional to square of n_T, and that impact on output current ripple [1].

$$L = \frac{V_{DC}/(N_L-1)}{8 \cdot f_s \cdot \Delta i_s} \tag{19}$$

Hair-pin winding technology is beneficial in terms of power density, thermal performance, and electromagnetic force with high slot fill factor and low slot openings [16]. In contrast, limited n_T is feasible for given number of poles and slots since even number of layer per slot are essential to hair-pin winding. For given same ratio of pole/slot combination, by increasing n_p, not only the power density increase, but higher n_T close to the optimal value following equation (18) can be designed shown in Table IV.

Table IV: Number of series turns per phase in hair-pin design depending on pole/slots

pole	slot	Layer per slot	Parallel circuit	Series turns per phase
8	48	4	1	32
	48	6	1	48
	48	8	2	32
10	60	4	1	40
	60	6	2	30
	60	8	2	40
12	72	4	1	48
	72	6	2	36
	72	8	2	48

Improved design and results

In this section, improved design is proposed in the way covered in the previous section. In Table V, design variables of machine design are described. Despite the increase in n_T, increasing n_p leads to decrease copper weight with lower phase current; that means proposed model has more higher power density.

Table V: Comparison of machine design

Item	Current Design	Improve Design
Image	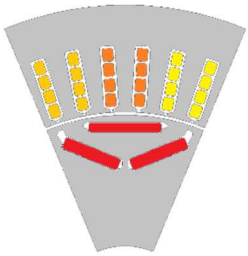	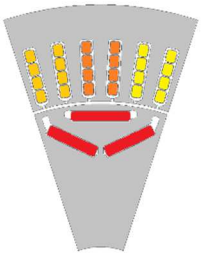
Pole / Slot	8 / 48	10 / 60
Outer diameter / Stack length [mm]	130 / 55	
Number of turns per phase	32	40
Magnet weight [p.u]	1.0	1.0
Copper weight [p.u]	1.0	0.90

For the inverter variable, the optimal switching frequency is 30kHz as the target of less than 5% of THD in the entire operation load point. Despite the loss reduction using 3L-ANPC topology, the use of higher switching frequency compared to 10kHz that is the value of original design has resulted in a slight increase in inverter loss. However, in terms of machine losses, the energy loss is improved. This is particularly evident in high-speed region where improvements in current waveforms are distinct. As a result, using All-SiC topology offers 20.7% reduction of total energy loss during driving cycle, even in hybrid topology, it has total 5.6% of energy savings shown in Table VII.

Table VI: Comparison of inverter and machine loss at each load point

Load point	Time [sec.]	Speed [rpm]	Torque [Nm]	Inverter Loss [W]			Machine Loss [W]		
				Original	Improve (All SiC)	Improve (Hybrid)	Original	Improve (All SiC)	Improve (Hybrid)
1	1.2	1640.9	21.2	211.5	219.6	376.2	522.1	510.1	511.7
2	2.7	1342.4	48.3	888.6	975.0	1504.9	2561.7	2380.1	2374.3
3	8.6	5815.1	-44.5	671.6	836.7	1229.8	2186.2	2090.7	2090.4
4	12.9	11215.9	-11.9	85.6	123.5	193.6	582.2	402.8	404.6
5	22.4	2094.8	-8.6	57.1	71.1	129.3	102.1	99.4	99.9
6	36.6	9186.7	-3.3	20.4	23.4	42.0	222.8	112.1	112.8
7	42	7789.6	-5.9	38.4	48.5	84.4	286.9	134.8	134.3
8	77.9	6490.6	-6.0	38.9	48.9	86.0	215.1	114.8	114.5
9	195	5105.2	-4.5	27.4	32.7	59.4	102.6	68.7	68.0
10	200.7	0.0	0.0	0.0	0.0	0.0	0.0	0.0	0.0

Table VII: Comparison of energy loss during driving cycle

Load point	Time [sec.]	Speed [rpm]	Torque [Nm]	Energy loss [kJ]		
				Original	Improve (All SiC)	Improve (Hybrid)
1	1.2	1640.9	21.2	0.9	0.9	1.1
2	2.7	1342.4	48.3	9.3	9.1	10.5
3	8.6	5815.1	-44.5	24.6	25.2	28.6
4	12.9	11215.9	-11.9	8.6	6.8	7.7
5	22.4	2094.8	-8.6	3.6	3.8	5.1
6	36.6	9186.7	-3.3	8.9	5.0	5.7
7	42	7789.6	-5.9	13.7	7.7	9.2
8	77.9	6490.6	-6.0	19.8	12.7	15.6
9	195	5105.2	-4.5	25.4	19.8	24.8
10	200.7	0.0	0.0	0.0	0.0	0.0
Total energy loss during driving cycle [kJ]				114.7	90.9 (20.7%↓)	108.3 (5.6%↓)

Conclusion

This paper has proposed the development of a comprehensive framework for joint inverter-machine co-design. The impact analysis is studied with important design parameters such as switching frequency, the number of level with 3L-ANPC topology, PWM strategies and machine pole number and turns. With simulation model based on analytic approach, the optimum design variable can be selected. A key figure-of-merit is energy efficiency considering total energy loss consumption of driving cycle. The effect of these design variables on energy loss vary depending on the application and driving condition. However, this methodology can be applied to the design of other EDs for EVs and HEVs.

References

[1] E. Gurpinar and A. Castellazzi: Tradeoff Study of Heat Sink and Output Filter Volume in a GaN HEMT Based Single-Phase Inverter, IEEE Transactions on Power Electronics, Vol. 33 no 6, pp. 5226-5239, June 2018, doi: 10.1109/TPEL.2017.2730038.

[2] S. Ozdemir, F. Acar and U. S. Selamogullari: Comparison of silicon carbide MOSFET and IGBT based electric vehicle traction inverters, 2015 International Conference on Electrical Engineering and Informatics (ICEEI), 2015, pp. 1-4, doi: 10.1109/ICEEI.2015.7387215.

[3] A. Allca-Pekarovic, P. J. Kollmeyer, P. Mahvelatishamsabadi, T. Mirfakhrai, P. Naghshtabrizi and A. Emadi: Comparison of IGBT and SiC Inverter Loss for 400V and 800V DC Bus Electric Vehicle Drivetrains, 2020 IEEE Energy Conversion Congress and Exposition (ECCE), 2020, pp. 6338-6344, doi: 10.1109/ECCE44975.2020.9236202.

[4] Z. Feng, X. Zhang, S. Yu and J. Zhuang: Comparative Study of 2SiC&4Si Hybrid Configuration Schemes in ANPC Inverter, IEEE Access, Vol. 8, pp. 33934-33943, 2020, doi: 10.1109/ACCESS.2020.2974554.

[5] A. Kersten, E. Grunditz and T. Thiringer: Efficiency of Active Three-Level and Five-Level NPC Inverters Compared to a Two-Level Inverter in a Vehicle, 2018 20th European Conference on Power Electronics and Applications (EPE'18 ECCE Europe), 2018, pp. P.1-P.9

[6] L. Zhang et al.: Evaluation of Different Si/SiC Hybrid Three-Level Active NPC Inverters for High Power Density, IEEE Transactions on Power Electronics, Vol. 35, no. 8, pp. 8224-8236, Aug. 2020, doi: 10.1109/TPEL.2019.2962907.

[7] Kim, DM., Jung, YH., Cha, KS. et al.: Design of Traction Motor for Mitigating Energy Consumption of Light Electric Vehicle Considering Material Properties and Drive Cycles, International Journal of Automotive Technology, Vol. 21, pp. 1391–1399, doi: 10.1007/s12239-020-0131-7

[8] K. T. Chau, C. C. Chan and C. Liu: Overview of Permanent-Magnet Brushless Drives for Electric and Hybrid Electric Vehicles, IEEE Transactions on Industrial Electronics, Vol. 55, no. 6, pp. 2246-2257, June 2008, doi: 10.1109/TIE.2008.918403.

[9] S. Xue et al.: Iron Loss Model for Electrical Machine Fed by Low Switching Frequency Inverter, IEEE Transactions on Magnetics, vol. 53, no. 11, pp. 1-4, Nov. 2017, Art no. 2801004, doi: 10.1109/TMAG.2017.2696360.

[10] K. Yamazaki and S. Watari: Loss analysis of permanent-magnet motor considering carrier harmonics of PWM inverter using combination of 2-D and 3-D finite-element method, IEEE Transactions on Magnetics, Vol. 41, no. 5, pp. 1980-1983, May 2005, doi: 10.1109/TMAG.2005.846278.

[11] K. Yamaguchi, K. Katsura and T. Jikumaru: Motor loss and temperature reduction with high switching frequency SiC-based inverters, 2017 IEEE 5th Workshop on Wide Bandgap Power Devices and Applications (WiPDA), 2017, pp. 127-131, doi: 10.1109/WiPDA.2017.8170534.

[12] Dong Wei, Hongwen He, Jianfei Cao: Hybrid electric vehicle electric motors for optimum energy efficiency: A computationally efficient design, Energy, Vol. 203, 2020, doi: 10.1016/j.energy.2020.117779

[13] J. W. Chin, K. S. Cha, J. C. Park, D. M. Kim, J. P. Hong and M. S. Lim: Investigation of AC Resistance on Winding Conductors in Slot According to Strands Configuration, IEEE Transactions on Industry Applications, Vol. 57, no. 1, pp. 316-326, Jan.-Feb. 2021, doi: 10.1109/TIA.2020.3033815.

[14] G. Artetxe, J. Paredes, B. Prieto, M. Martinez-Iturralde, and I. Elosegui: Optimal Pole Number and Winding Designs for Low Speed–High Torque Synchronous Reluctance Machines, Energies, Vol. 11, no. 1, p. 128, Jan. 2018, doi: 10.3390/en11010128.

[15] D. Misu, M. Matsushita, K. Takeuchi, K. Oishi and M. Kawamura: Consideration of optimal number of poles and frequency for high-efficiency permanent magnet motor, 2014 International Power Electronics Conference (IPEC-Hiroshima 2014 - ECCE ASIA), 2014, pp. 3012-3017, doi: 10.1109/IPEC.2014.6870113.

[16] G. Berardi, S. Nategh, N. Bianchi and Y. Thioliere: A Comparison Between Random and Hairpin Winding in E-mobility Applications, IECON 2020 The 46th Annual Conference of the IEEE Industrial Electronics Society, 2020, pp. 815-820, doi: 10.1109/IECON43393.2020.9255269.